

Comparative Analysis of Magnetic Slot Wedges Design for Increasing Performance of Railway Traction Motor

Huai-Cong Liu*, Sooyoung Cho*, Hyun-Seok Hong*, Kyoung-Jin Joo*, Sang-Hwan Ham** and Ju Lee†

Abstract – This study focuses on the effects of using open stator slots in an interior permanent magnet traction motor with a magnetic slot wedge design in order to increase the power density at its base speed. In addition, such a configuration reduces the torque ripple under field-weakening conditions. Five different wedge models were selected, each of which was evaluated using a finite element analysis (FEA). Based on the initial model, we designed magnetic slot wedges for maximum back-EMF and minimum cogging torque. In addition, the d-q axis inductance was slightly altered due to the magnetic slot wedges. Finally, we analyzed the performance of a traction machine under field weakening control. Moreover, we have outlined the requirements for an ideal magnetic slot wedge design.

Keywords: Light rail transit, Magnetic slot wedge, Tram-train, Traction motor, Cogging torque, Torque density

1. Introduction

Recently, railroad cars – specifically, light rail transit (LRT) – have been proposed as solutions to both traffic problems and environmental problems. LRT has proven to be superior to subways in terms of construction costs and accessibility. In particular, a tram-train can be operated on common roads and requires much fewer construction costs [1]. Further, a tram-train can be utilized as a semi-high-speed train to connect cities.

A crucial characteristic of the tram-train is that it can be driven in both urban and rural areas, running at a maximum speed of 70km/h in urban areas and 150km/h between cities. Therefore, the operating point varies due to differences in departure acceleration. Depending on each operation pattern, traction may or may not be required by each traction motor [2]. Thus, the required traction for each tram and train torque/speed curves, respectively, must be considered. Fig. 1 shows the required traction curve in the tram and train intervals, respectively. Permanent magnet (PM) motors are considered to be the best solution to fit this type of load curve.

In particular, an interior permanent magnet synchronous motor (IPMSM) using rare-earth magnet, such as neodymium iron boron (NdFeB), may provide a high torque density and high-efficiency solution for such demanding

applications as the tram-train automotive system. IPMSMs have been developed to improve the efficiency and output density of a tram-train system, in comparison to induction motors. The trend has been to design a tram-train's IPMSM to be free of vibration and acoustic noise in order to obtain smooth torque with minimum pulsation an accurate positional control. Doing so also improves passengers' overall comfort levels [3,4].

A parallel slot is usually used to improve the slot fill factor in order to achieve a higher torque density at base-speed, with an integral-slot distributed winding. In this case, the motor's tooth tips were narrower than their bottoms, and the flux density in the tooth tips often exceeded 2T under rated working conditions. Here, the unbalanced air-gap flux density produced very large slot harmonics and torque ripples.

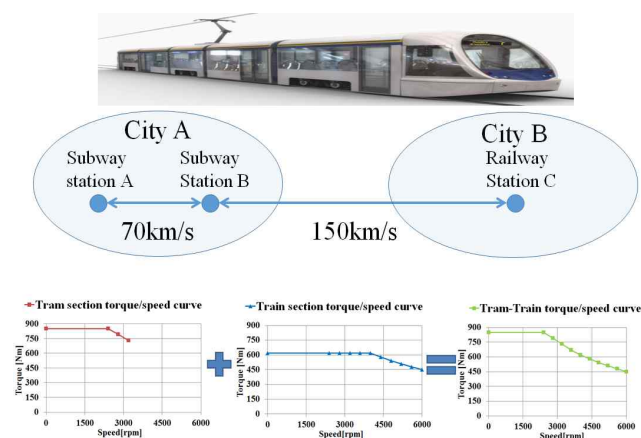


Fig. 1. Required traction curve of a traction motor for a tram-train system-

† Corresponding Author: Dept. of Electrical and Electronic Engineering, Hanyang University, Korea. (julee@hanyang.ac.kr)

* Dept. of Electrical and Electronic Engineering, Hanyang University, Korea. (liu1988@msn.com, jsy0593@naver.com, hhs0321@gmail.com, kj8532@hanyang.ac.kr)

** Dept. of Electrical and Railway Engineering, Kyungil University, Korea. (shham@kiu.kr)

Received: January 13, 2017; Accepted: June 22, 2017

In this situation, the magnetic slot wedge will reduce the saturation in the tooth tip. This function could counteract the torque reduction caused by slot leakage, thereby decreasing the cogging torque and torque ripple, an eliminating torque reduction.

In previous studies, cogging torque was a major concern in PM motors [5-9]. Although a magnetic wedge application for axial flux machines has been mentioned [10], it was different from pre-formed radial flux PM machines.

This paper presents a novel magnetic wedge shape consisting of double-layer and multi-layer types for a tram-train system IPMSM. The proposed magnetic wedge shape was designed for a fundamental waveform of back-EMF, which would yield a favorable combination of wedge reduction and back electromotive force (back-EMF) harmonics. A detailed 2-D finite element analysis (FEA) for the five models was conducted as a comparison of the magnetic field distribution and flux line distribution results at a no-load state, start point, and field weakening point. Section II discusses the modeling of the IPMSM in detail, and Sections III contains a comparison of both the 2-D FEA results for open circuit and load operation. Finally, concluding remarks are given in Section IV.

2. Modeling of IPMSM with Magnetic Slot Wedge Design

2.1 Tram-train system IPMSM and torque characteristics

This project presents the 210-kW class three-phases IPMSM with the six-pole/ fifty four-slot structure. As for the PM geometrical arrangement, the rotor PMs can be positioned as “_”, “V” and “_/”. The “_/”-shape PMs can offer a highest flux density than the other shapes”. a “_/”-shape PM arrangement is chosen in this work. Firstly, the sizing of the machine is conducted and its performance is investigated including the flux density, self- and mutual-inductances, electrical torque and torque ripple by the FEM. The rotor barrier, shape and geometry of PMs are

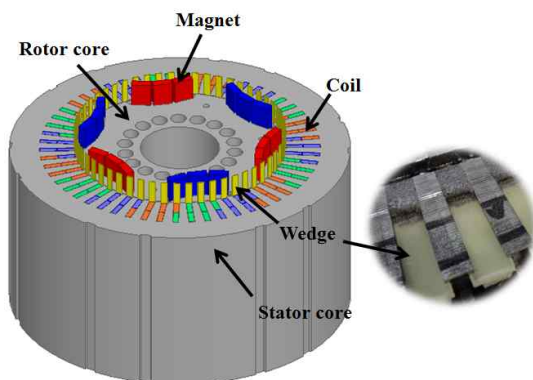


Fig. 2. Configuration of the basic model (Model 1)

Table 1. Specifications of basic models

Item	Unit	Value
Rated power	kW	210
Maximum power	kW	282
Rated speed	rpm	2400
Maximum speed	rpm	6000
Magnet poles/Stator slots	-	6/54
Stator outer diameter	mm	430
Rotor outer diameter	mm	260
Rotor inner diameter	mm	100
Air-gap length	mm	1.5
Permanent magnet thickness	mm	10
Permanent magnet length	mm	24
Lamination axial length	mm	220

based on the previous work where several optimization methods are exercised to enhance the motor performance (torque density, spatial harmonics and cogging torque). After optimization, the design parameters are obtained, as presented in Table 1.

The rotor and stator lamination indicating the location of the sintered rare-earth rotor magnets is shown in Fig. 2. The machine had high iron loss in the stator teeth. Cutting the tips of the stator teeth to form open slots reduced this effect, indicating that the stator slot openings were widened. Here, using open slots will have implications for the mechanical retention of the windings in the slots. The basic model contains non-magnetic wedges to prevent the winding dropout and increase the mechanical strength. Meanwhile, the inner holes in the rotor are used to make a cooling loop, reduce the motor temperature in the overload operation.

2.2 Proposed model: Open slots IPMSM with different wedge design models

A glass-fiber non-magnetic wedge was used as a reference wedge material. Its relative permeability was equal to 1, and it did not cause heat or other losses; hence, the resistivity may be assumed to be infinite. Fig. 4(a) shows the glass-fiber wedges assembled in a basic 210 kW model. Some other materials in the closings of the slot opening were magnetic wedges with a relative permeability ranging from 1 to 850. Magnetic wedges with a relative perme-

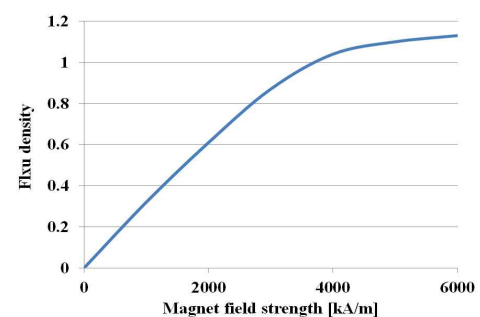


Fig. 3. The magnetization (B/H) curves of the magnetic slot wedges

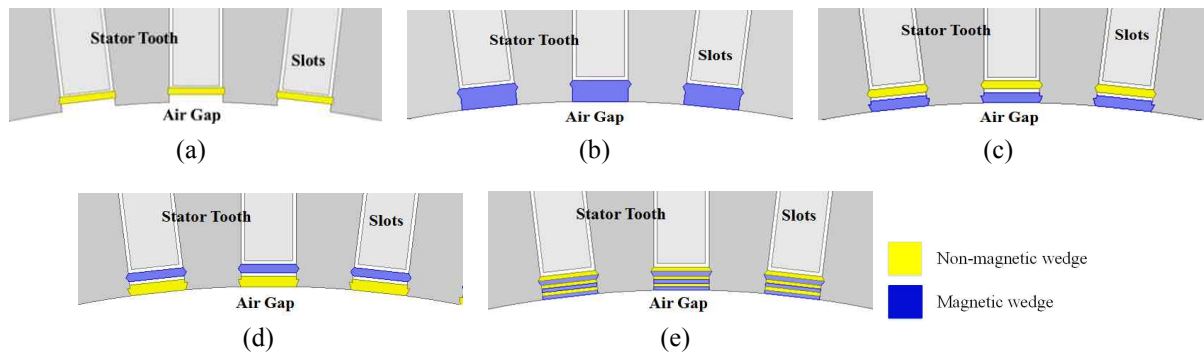


Fig. 4. Comparison of magnetic and non-magnetic wedge design models. (a) Basic model (Model 1); (b) Model 2; (c) Model 3; (d) Model 4; (e) Model 5.

ability from 1 to 7 (e.g. Magnoval) are generally made of glass cloth (5-10%), iron powder (75%), and a high temperature-resistant epoxy resin (15-20%). The model's magnetization (B/H) curves can be seen in Fig. 3.

Another four magnetic wedge structures are described in Fig. 4(b)-(d). Fig. 4(a) shows a basic model with the most typical non-magnetic wedge design. Fig. 4(b) contains a magnetic slot wedge, compared to the traditional open slot structure. Fig. 4(c) double layer wedge: contains a magnetic wedge to under the non-magnetic slot wedge; whereas, the model in Fig. 4(d) has a magnetic and non-magnetic wedge in a different position. Fig. 4(e) shows a multi-layer slot wedge designed to reduce eddy current loss from the magnetic wedge.

The open-slot design has larger stator slot openings, hence, a larger Carter's coefficient than the original semi-closed design. This results in an increase of the effective air gap in the machine, thereby reducing the open-circuit air gap flux density. In turn, this configuration reduces the back-EMF voltage hence, the PM contribution of the output torque.

3. FEM Analysis of IPMSM with Five Magnetic Wedge Models

3.1 No-load back-EMF and cogging torque analysis

The open-slot design has larger stator slot openings hence, a larger Carter's coefficient than the original semi-closed design. This results in an increase of the effective air gap in the machine, thereby reducing the open-circuit air gap flux density. In turn, this configuration reduces the back-EMF voltage – hence, the PM contribution of the output torque.

The phase of the no-load back-EMFs of the five models is shown in Fig. 5. Due to the same rotation speed (2400 rpm), the root mean square (RMS) values of the no-load back EMF are kept the same in all five models to enable a reasonable comparison of EMF harmonics and torque pulsations. The basic models showed no-load back-EMF

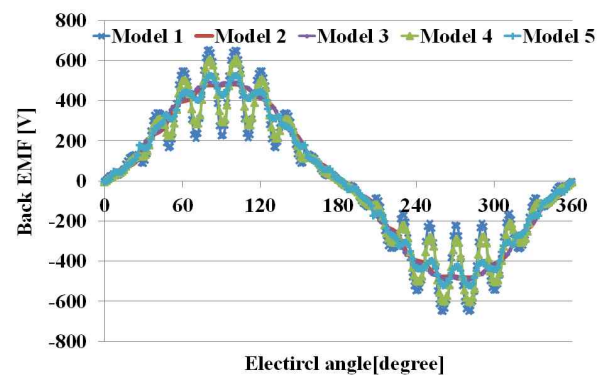


Fig. 5. Phase back-EMFs for all five models

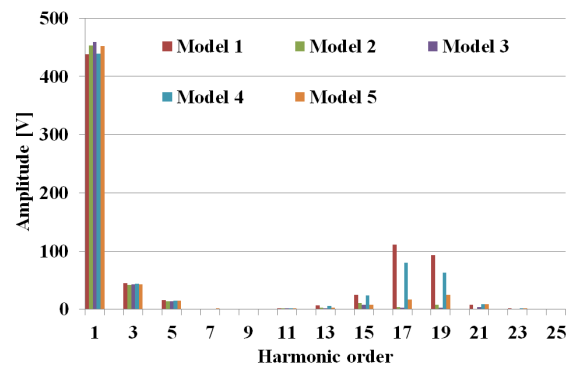


Fig. 6. FFT analysis of the phase back-EMFs

waveforms that consisted mainly of harmonics, while model 2 and model 3 exhibited good sinusoidal back-EMF waveforms. A fast Fourier transform (FFT) analysis of back-EMFs is shown in Fig. 6, to evaluate the sinusoidal quality of the back-EMF

The basic model caused a small relative drop in the fundamental component of the back-EMF, and a substantial relative increase in the higher harmonics - in particular, the 17th and 19th. This was expected, given that these correspond to the lowest-frequency tooth harmonics. A higher tooth-slot permeability variation among the open slots was expected to increase the magnitude of these harmonic components.

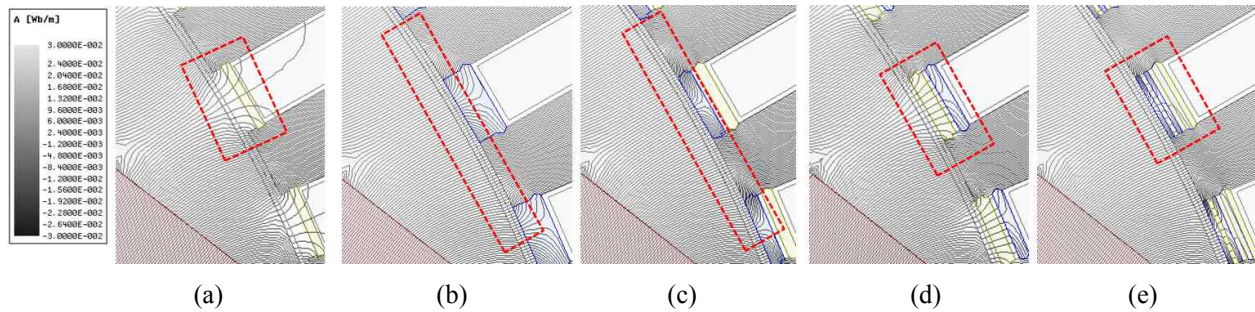


Fig. 7. Open circuit flux line field distribution: (a) Model 1; (b) Model 2; (c) Model 3; (d) Model 4; (e) Model 5

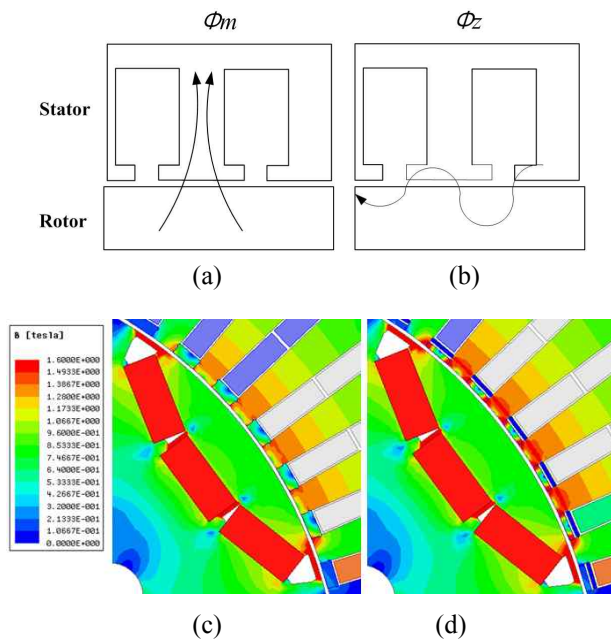


Fig. 8. Magnetic flux path in IPMSM (a) Main flux path at no-load; (b) Zig-zag leakage flux path for a locked rotor, and open circuit magnetic field distribution; (c) Model 2; (d) Model 3

Fig. 7 shows the open circuit flux line field distribution for the five models. In the case of model 2, model 3, and model 5, the flux transfer between the stator teeth could be smoothed, thereby reducing the 17th and 19th harmonics. However, in the case of model 5, the magnetic slot wedge closest to the air-gap was too narrow and magnetic saturation occurred, which yielded an insignificant reduction in the 17th and 19th in model 4.

Since the magnetic wedge was located too far from the air-gap, the fringing effect resulted in no significant improvements in air-gap flux.

Model 2 and model 3 contain almost solely a fundamental component of back-EMFs due to their proposed magnetic wedge shape design, without any complex optimization procedures. The harmonic distortions (THDs) of the back-EMFs of the four models were 34.50%, 7.25%, 7.75%, 24.60%, and 10.82%, respectively, which are calculated using

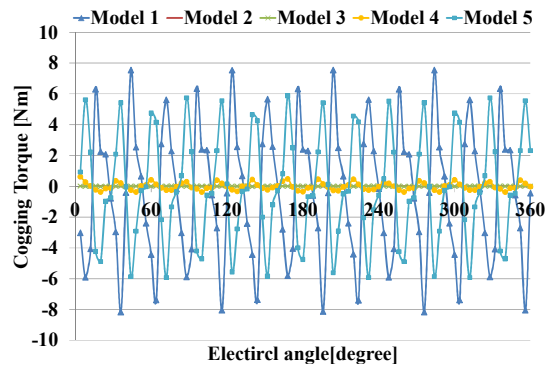


Fig. 9. Comparison of cogging torque

$$THD = \frac{\sqrt{E_2^2 + E_3^2 + E_4^2 + \dots}}{E_1} \quad (1)$$

Model 3 exhibited a superior sinusoidal back-EMF waveform than model 2 because the fundamental back EMF of model 3 was larger than that of model 2. Fig. 8 shows the open circuit magnetic field distribution for model 2 and model 3. Even though both model 2 and model 3 could reduce the saturation in the tooth tip, model 2's magnetic wedge was too wide; thus, zig-zag leakage flux was increased, which reduced the air-gap flux density.

Hence, an even better sinusoidal back-EMF waveform was expected when the radial width of the wedges was designed to be 1~2mm for the basic model, which indicated an 'ease of manufacturing' issue. Fig. 9 shows a comparison of the cogging torque between the five models. Model 3 showed the least peak-to-peak value for cogging torque (0.5 Nm), which was 15Nm, 0.1Nm, 0.6Nm, and 11.2Nm less than those of model 1, model 2, model 4, and model 5, respectively. It should be mentioned here that model 3 had the best magnetic slot wedge width and position, and it can be concluded that the wedge design was the main contributor to the model's reduction of cogging torque.

3.2 Electromagnetic torque and magnetic slot wedge performance on the load operation

Sinusoidal current excitation has been utilized to evaluate

Table 2. Two-dimensional FEA results

Item	Unit	Model 1	Model 2	Model 3	Model 4	Model 5
Open circuit analysis @ 2400rpm						
Phase back EMF @2400rpm	V	327.9	321.0	323.7	319.4	320.6
THD of back EMF	%	34.5	7.2	7.7	24.6	10.8
Cogging torque	Nm	15.7	0.5	0.6	1.1	11.7
Load operation @ 2400rpm (Start point) , Target torque: 850 Nm, MTPA						
Current angle	Deg	42	45	45	42	42
Average torque	Nm	853.2	840.9	862.3	812.4	839.1
Torque ripple factor	%	11.6	6.31	8.5	6.0	9.5
Output power	kW	214.4	211.3	216.7	204.1	210.9
Copper loss	W	2847.7	2847.7	2847.7	2847.7	2847.7
Iron loss	W	1970.5	2030.4	1928.6	1972.1	1914.2
Eddy current loss (Magnet)	W	74.2	82.2	75.5	78.3	76.2
Eddy current loss (Magnet wedge)	W	-	912.9	441.7	309.6	406.3
Efficiency	%	97.8	97.7	97.8	97.7	97.8
Load operation @ 6000rpm (Maximum speed point) , Target torque: 450 Nm, field weakening						
Current angle	Deg	74	74	74	74	74
Average torque	Nm	445.0	453.9	464.4	416.5	445.6
Torque ripple factor	%	45.7	22.9	24.2	29.8	26.4
Output power	kW	279.6	285.2	291.8	261.7	280.0
Copper loss	W	2847.7	2847.7	2847.7	2847.7	2847.7
Iron loss	W	6523.1	7002.4	6482.3	6161.5	6211.0
Eddy current loss (Magnet)	W	133.8	158.2	127.5	145.5	139.2
Eddy current loss (Magnet wedge)	W	-	2795.7	1379.3	882.4	1209.7
Efficiency	%	96.7	96.6	96.9	96.6	96.8

the electromagnetic torque characteristics of the five proposed models. The target electromagnetic torque at a starting rotational speed of 2400 r/min is 850Nm and maximum speed of 6000r/min was 450Nm (Fig. 1). The average output torque of the five models was approximately the same. Moreover, basic model 3 was regarded as the preferred reference model rather than basic model 1, since it had the largest power density, thereby providing the same operating point comparison. The torque ripple factor was defined as the ratio of the peak-to-peak torque value to the average torque value, and was adopted for torque ripple calculations using

$$K_T = \frac{T_{\max} - T_{\min}}{T_{\text{avg}}} \quad (2)$$

The comparison results are summarized in Table 3. We used MAXWELL software to evaluate the iron loss accurately, considering nonlinear phenomena, based on the following equation:

$$P_{\text{iron}} = \sum_i^{Nelement} [P_{h_i}(B, f_e) + P_{e_i}(B, f_e)] \quad (3)$$

The eddy current loss from the magnetic wedge consistently varied according to the thickness of the magnetic wedge. Thus, model 5 had the best performance when the thickness of each wedge layer was smallest.

The copper loss can be found by

$$P_{\text{copper}} = 3I_{\text{rms}}^2 R \quad (4)$$

Although the copper loss in model 4 was the highest, it still maintained similar efficiency to the other three models due to a reduction of iron loss. The efficiency of the models can be defined by

$$\eta = \frac{P_{\text{out}}}{P_{\text{out}} + P_{\text{copper}} + P_{\text{iron}}} \quad (5)$$

Where the output power P_{out} is obtained by

$$P_{\text{out}} = T_e \frac{2\pi\omega_r}{60} \quad (6)$$

Here, a larger effective air gap in the magnetic slot wedge increased the inductances in both the d- and q-axes of the machine, which affected the reluctance contribution of the output torque. The machine without a magnetic slot wedge had high electric and magnetic loading, exhibiting strong saturation at the teeth.

Fig. 10(a) shows a comparison of model 3 and model 1 in terms of the calculated FEA d-q axis inductances changes to model 3 increased the induction in the d-q axis at a 42deg, 220Apeak from 1.78mH, 5.94mH to 2.37mH, 6.50mH. Secondly, at the field-weakening point (6000rpm), the strong magnetic flux from the rare-earth magnets was reduced by the stator current, which reduced the d-q axis saturation of the stator magnetic wedge, as well as the q-axis saturation of the web. This process also caused the q-axis inductance to increase much more than that of the baseline starting point. Fig. 10(b) presents the calculated torque against current angle curves for model 1 and model

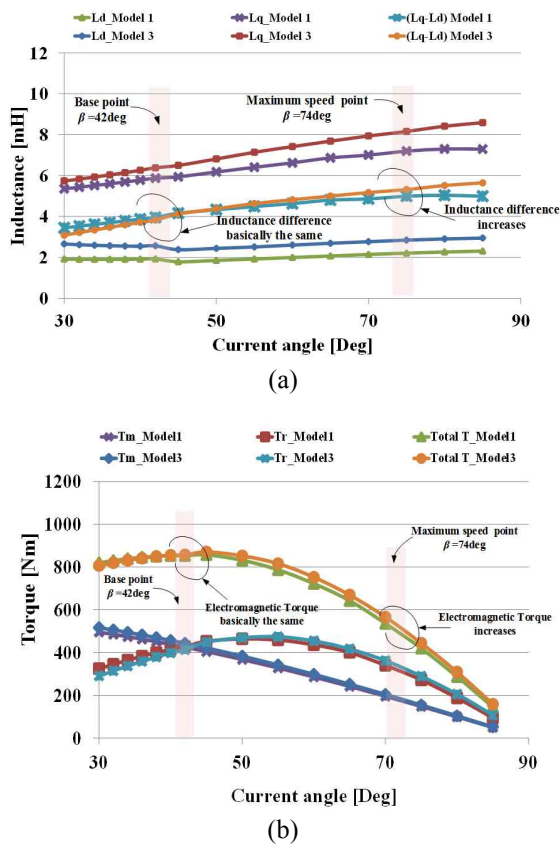


Fig. 10. Calculated electromagnetic torque against current angle, based on inductance saturation curves, using calculated parameters (FEA) for model 1 and model 3: (a) Current angle/inductance curve; (b) current angle/torque curve

3. Because of the increase in q-axis inductance, the IPMSM had significantly improved power and efficiency at high speed operation.

4. Conclusion

In this paper, four magnetic slot wedge shapes were proposed to minimize torque pulsation. The proposed wedge shape was designed for a fundamental waveform of back-EMF. The design achieved a superior combination of saturation by reducing the number of teeth and minimizing the back-EMF harmonics. In order to facilitate the ease of manufacturing, the proposed wedge shape was designed with 1 layer of non-magnetic materials and 1 layer of magnetic stacks, which enabled the back-EMF to approximate a sine wave. A detailed 2-D FEA prediction of salient characteristics for the five models was illustrated by comparison results. The following conclusions can be obtained from these results.

The open slot IPMSM with a magnetic wedge in the axial direction between teeth could produce a nearly sinusoidal back-EMF waveform. Model 3 appeared to

have a superior sinusoidal back-EMF waveform with fewer harmonic components than other models.

Model 3 had 1 layer of non-magnetic materials and 1 layer of magnetic stacks. This configuration was a prominent advantage for large power density at high speeds, especially in the tram-train system applications, which required precise positional control in applications such as traction and brake systems.

The open slot IPMSM with magnetic wedges could effectively minimize the torque pulsation. The proposed model 3 significantly reduced not only cogging torque, but also torque ripple.

At the high-speed field-weakening control point, the IPMSM for model 3's q-axis inductance of saturation decreased, thereby increasing the torque density.

The design of the magnetic wedge will engender some additional eddy current loss. In order to solve this problem, magnetic slot wedge lamination will reduce the eddy current loss; however, this will make manufacturing very difficult. Therefore, taking into account the safety of a motor's performance in reducing the additional eddy current loss will be the subject of future research.

Appendix

A.1 Experiment

The IPMSM basic model introduced in this paper was manufactured. And test equipment is shown in Fig. 11. Fig.

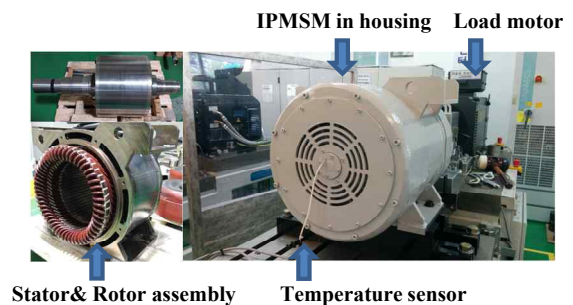


Fig. 11. Manufactured prototypes of basic IPMSM and test set

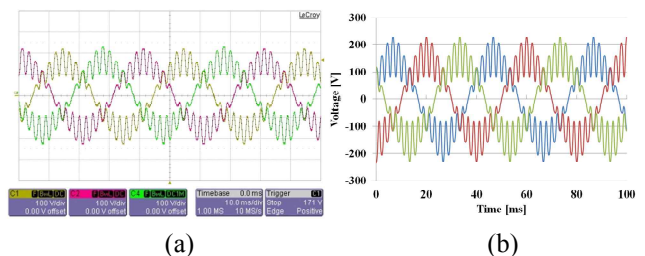
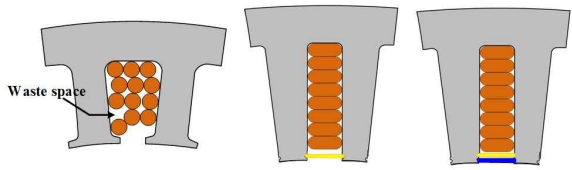


Fig. 12. Experiment and simulation results of no-load line-induced voltage at 500r/min: (a) Experiment; (b) Simulation

Table 3. Wedge costs and characteristics comparison


Item	Unit	Model 1	Model 2	Model 3
Cost	¥	0	47.5	237.6
Cogging torque	Nm	9.2	15.7	0.6
Fill factor	%	42	58	58

12 shows the experimental and simulation values of the no-load line-induced voltage at 500 r/min and 22°C in basic model (with no magnetic wedge). The experimental value of the no-load line-induced voltage is 120.3V, and the simulation value is 177.7V, which show that these two values are relatively similar.

A.2 Cost and characteristics

The quotation is based on the market price in 2017 in China:

- Cost of magnetic wedge: 0.8 ¥/50mm;
- Cost of Non-magnetic wedge: 0.2 ¥/50mm;

The material costs, cogging torque and fill factor of magnetic wedge, Non-magnetic wedge, and semi-closed IPMSM model are listed in Table 3. The price of magnetic wedge insert IPMSM is about 25% 22% higher than No-magnetic wedge IPMSM and semi-closed IPMSM model respectively. But cogging torque and fill factor of magnetic wedge insert IPMSM were greatly reduced. Magnetic wedge has great advantage over IPMSM in term of reducing cogging torque and increasing fill factor.

Acknowledgements

This research was supported by Basic Science Research Program through the National Research Foundation of Korea (NRF) funded by the Ministry of Education, Science and Technology (NRF-2017R1D1A1B03028427)

This work was supported by the Human Resources Program in Energy Technology of the Korea Institute of Energy Technology Evaluation and Planning (KETEP), granted financial resource from the Ministry of Trade, Industry & Energy, Republic of Korea. (No. 2015 4030200900).

References

- [1] R.E Kim, J.C Kim B.C Kim, Y.H Park, J.S Han, "Development of totally enclosed traction motor for

low floor tram", *The Korean Society for Railway spring conference*, pp. 1642-1646, 2011.

- [2] S.K. Yang, G.C. Jeong, H.C. Liu, C.B. Park, H.W. Lee, J. Lee, "A study on traction motor design for a Tram-Train which takes into consideration of a permanent magnet scattering", *ICEMS, 18th International Conference on* pp.1494-1497, 2015.
- [3] K. Kiyota and A. Chiba, "Design of switched reluctance motor competitive to 60-kW IPMSM in third -generation hybrid electric vehicle," *IEEE Trans. Ind. Appl.*, vol. 48, no. 6, pp. 2303-2309, Nov./Dec. 2012.
- [4] T. Kosaka, T. Hirose, and N. Matsui, "Experimental studies on drive performances of less rare-earth PM hybrid excitation motor," in *Proc. 8th IEEE ICPE ECCE*, pp. 161-168, Jun. 2011.
- [5] L. Zhu, S. Z. Jiang, Z. Q. Zhu, and C. C. Chan, "Analytical methods for minimizing cogging torque in permanent-magnet machines," *IEEE Trans. Magn.*, vol. 45, no. 4, pp. 2023-2031, Apr. 2009.
- [6] N. Bianchi and S. Bolognani, "Design techniques for reducing the cogging torque in surface-mounted PM motors", *IEEE Trans. Ind. Appl.*, vol. 38, no. 5, pp. 1259-1265, Sep. 2002.
- [7] G.W. Cho, W.S. Jang, K.B. Jang and G.T. Kim "The Optimal design of fractional-slot SPM to reduce cogging torque and vibration", *Journal of Electrical Engineering & Technology*, vol. 7, no. 5, pp. 753-758, Sep. 2012.
- [8] J. Hur, B.W. Kim "Rotor Shape Design of an Interior PM Type BLDC Motor for Improving Mechanical Vibration and EMI Characteristics" *Journal of Electrical Engineering & Technology* vol. 5, no. 3, pp. 462-467, May 2010.
- [9] S.J. K, E.J. Park, Y.J. Kim "Optimal design of ferromagnetic pole pieces for transmission torque ripple reduction in a magnetic-gear machine" *Journal of Electrical Engineering & Technology* vol. 6, no.11, pp. 1628-1633, Nov. 2016.
- [10] G. D. Donato, F. G. Capponi, and F. Caricchi, "On the use of magnetic wedges in axial flux permanent magnet machines", *IEEE Trans. Ind. Electro.*, vol. 60, no. 11, pp. 4831-4840, Nov. 2013.



Huai-Cong Liu He received the B.S. degree in electrical engineering from Chungnam national University, Daejeon, Korea in 2012, Since 2012, He has been pursuing the Ph.D. degree at the Department of Electrical Engineering, Hanyang University. His research interests include design, analysis, testing and control of motor/generator; power conversion systems; and applications of motor drive.



Sooyoung Cho She received the B.S. degree in electrical engineering from Myongji University, Yongin, Korea in 2013 and the M.S. degrees in electrical engineering from Hanyang University, Seoul, Korea in 2015. Since 2015, she has been pursuing the Ph.D. degree at the Department of Electrical Engineering, Hanyang University. Her research interests include design, analysis, testing and control of motor/generator; power conversion systems; and applications of motor drive.



Hyun-Seok Hong He received his B.S. degree in Electrical Engineering from Dankook University, Seoul, Korea in 2012 and M.S. degree in Electrical Engineering from Hanyang University, Seoul, Korea in 2014. Since 2014, he has been pursuing the Ph.D. degree at the Department of Electrical Engineering, Hanyang University. His research interests include design, analysis, testing and control of motor/generator; power conversion systems; and applications of motor drive.



Kyoung-Jin Joo She received her B.S. degree in Electrical Engineering from Changwon National University, Changwon, Korea in 2008, and her M.S. degree in Electrical Engineering from the same university, in 2010. She worked in Korea Electrotechnology Research Institute from 2010 to 2011 and LG electronics from 2011 to 2015. Since 2015, she has been pursuing the Ph.D. degree at the Department of Electrical Engineering, Hanyang University. Her research interests include design, analysis, testing and control of motor/generator; power conversion systems; and applications of motor drive, such as electric vehicles.



Sang-Hwan Ham He received his B.S., M.S. and Ph.D. degrees in Electrical Engineering from Hanyang University, Seoul, Korea in 2006, 2008 and 2011 respectively. He joined Kyungil University and is currently a Professor of the school of Electrical Engineering. His research interests include design, analysis of motor/generator.



Ju Lee He received his M.S. degree from Hanyang University, Seoul, South Korea, in 1988, and his Ph.D. from Kyusyu University, Japan in 1997, in Electrical Engineering. He joined Hanyang University in September 1997, and is currently a Professor of the Division of Electrical and Biomedical Engineering. His main research interests include electric machinery and its drives, electro-magnetic field analysis, new trans-formation systems such as hybrid electric vehicles (HEV), and high-speed electric trains and standardization. He is a member of the IEEE Industry Applications Society, Magnetics Society, and Power Electronics Society.